Supplementary material to Remote control of the retroflection of the Labrador Current

Mathilde Jutras, Carolina O. Dufour, Alfonso Mucci, Lauryn Talbot

A Additional figures

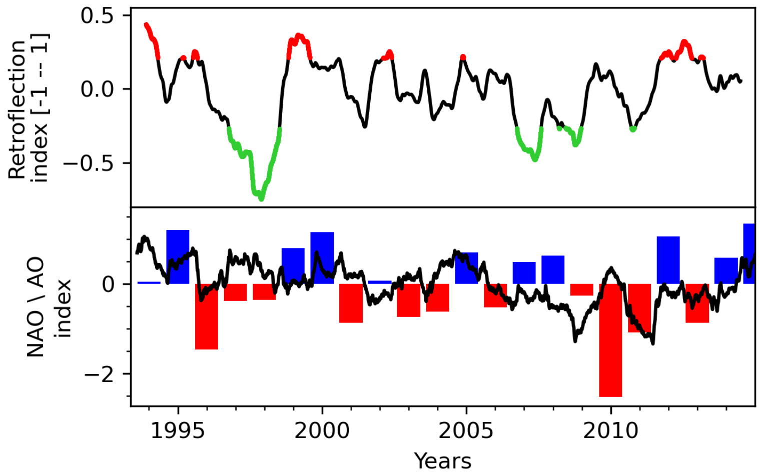

Figure S1: Comparison of the retroflection index (top panel, see Fig. 3) to the NAO (bars, bottom panel) and AO (black line, bottom panel) indices.

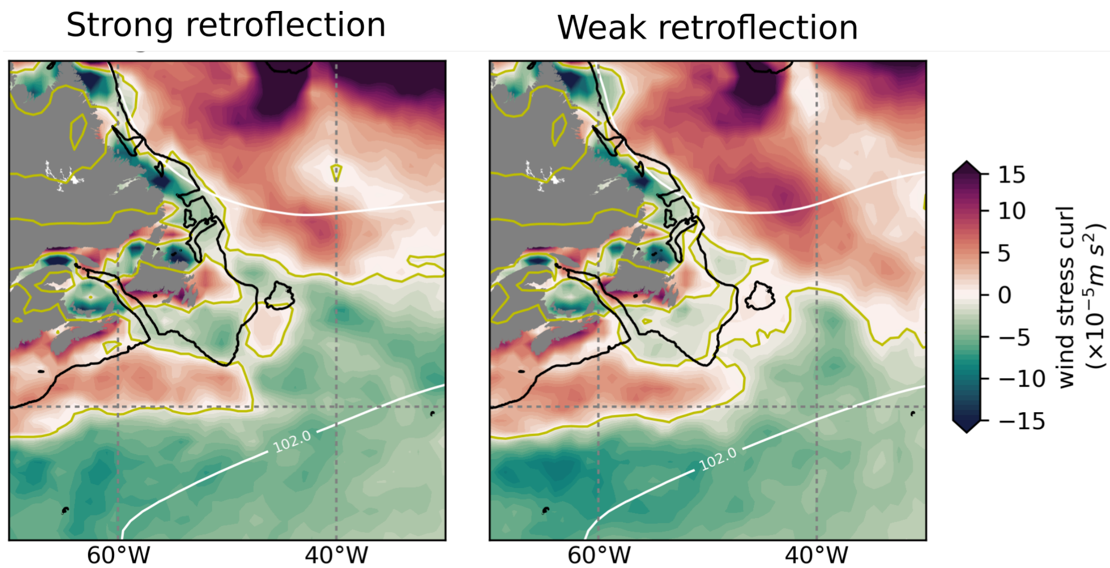

Figure S2: Composite maps of the wind stress curl. The yellow contours indicate the -0.5 wind stress curl lines, and highlight the connection between zones of positive wind stress curl during weak retroflection periods. The white contours are isolines of atmospheric pressure, in hPa. The black line delineates the 350 m isobath.

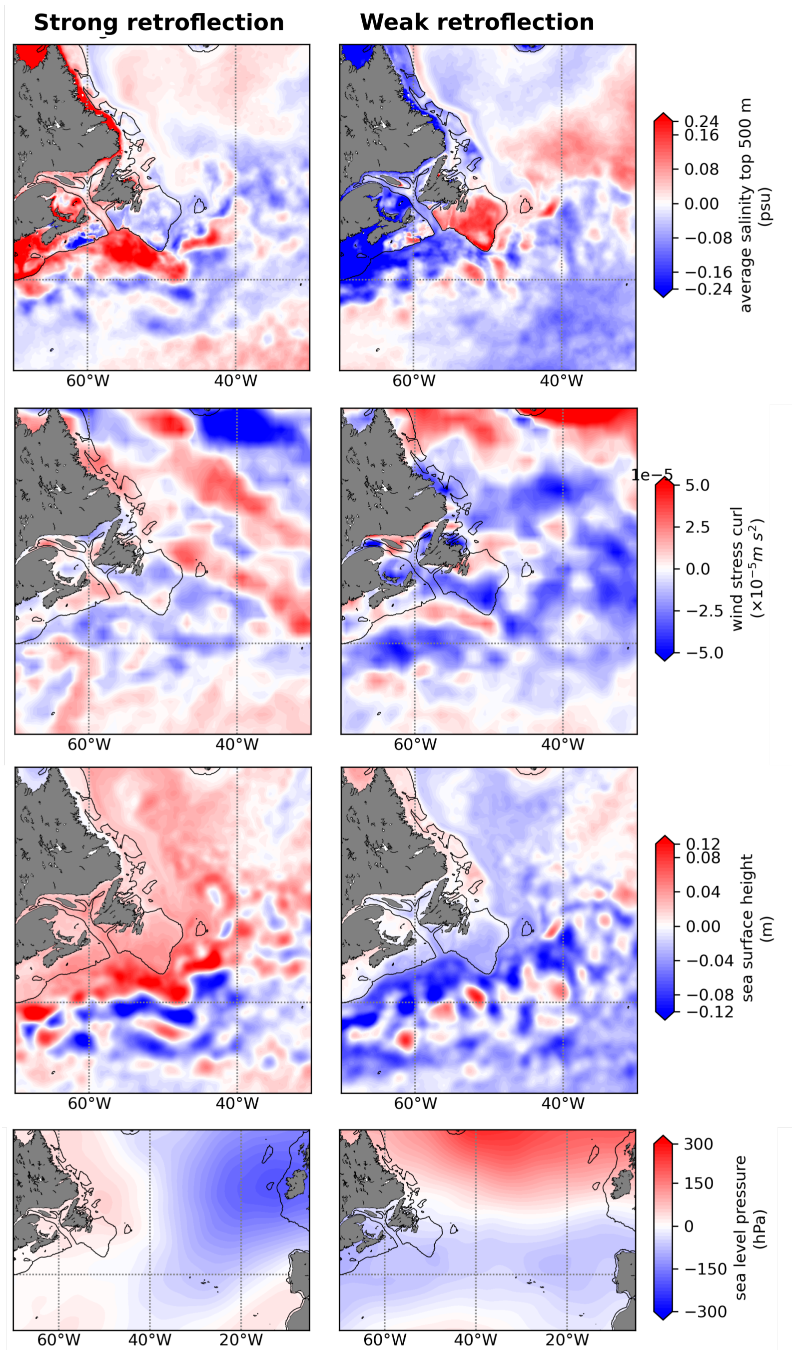

Figure S3: Composite maps in periods of strong (left) and weak (right) retroflection, for the anomalies of the same variables as Fig. 4. Composites are based on the periods identified in Fig. 3a. Note that the domain is different for the sea level pressure (g-h).

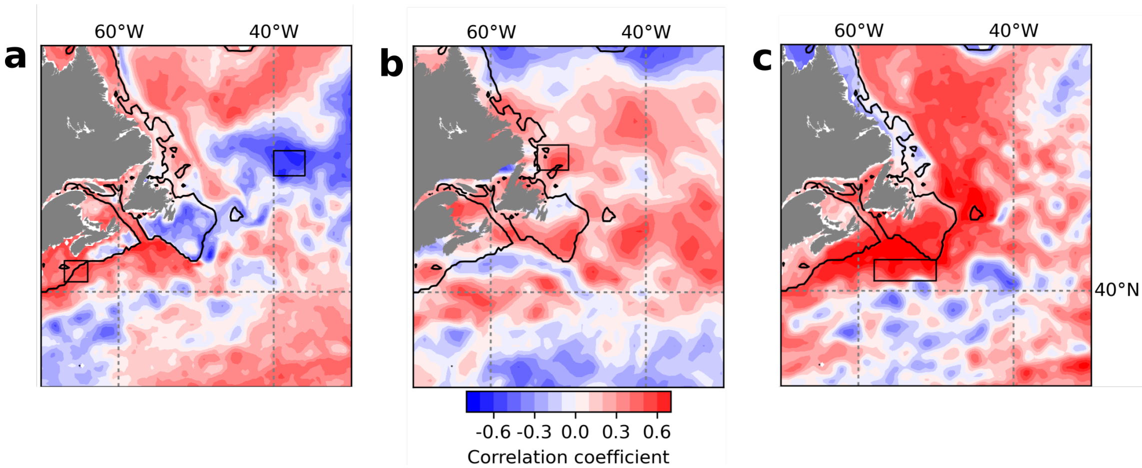

Figure S4: Correlation maps between the retroflection index and (a) average salinity in the top 500 m, (b) wind stress curl, and (c) sea surface height. The boxes show zones of strong correlation used to compute the time series of Fig. 3 for the different fields.

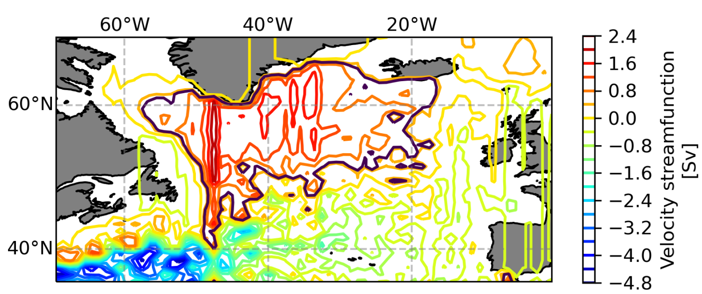

Figure S5: Barotropic quasi-streamfunction of the velocities in January 1993. The black contour delineates the area used for the calculation of the subpolar gyre index.

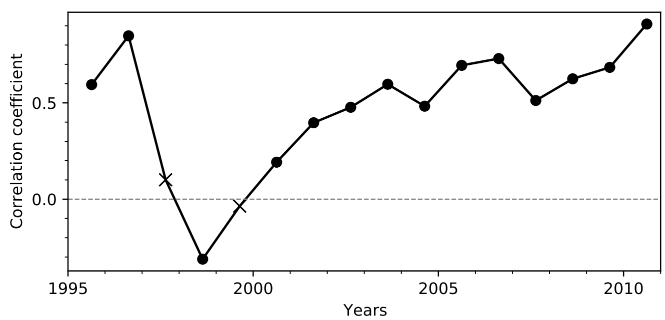

Figure S6: Correlation coefficient between the retroflection index and the volume transport of the Labrador Current, for 3-years segments. The dots indicate segments with significant correlations, and the crosses segments with non-significant correlations.

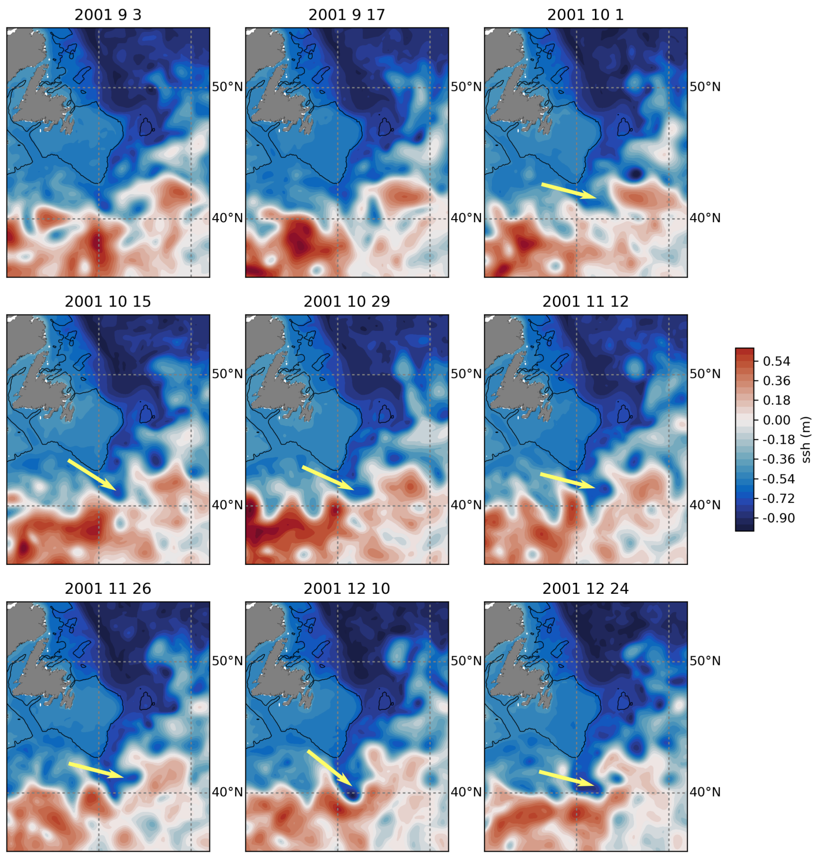

Figure S7: SSH maps showing the evolution of the formation of a cyclonic eddy (yellow arrow) at the tip of the Grand Banks from the tongue of Labrador Current Waters.

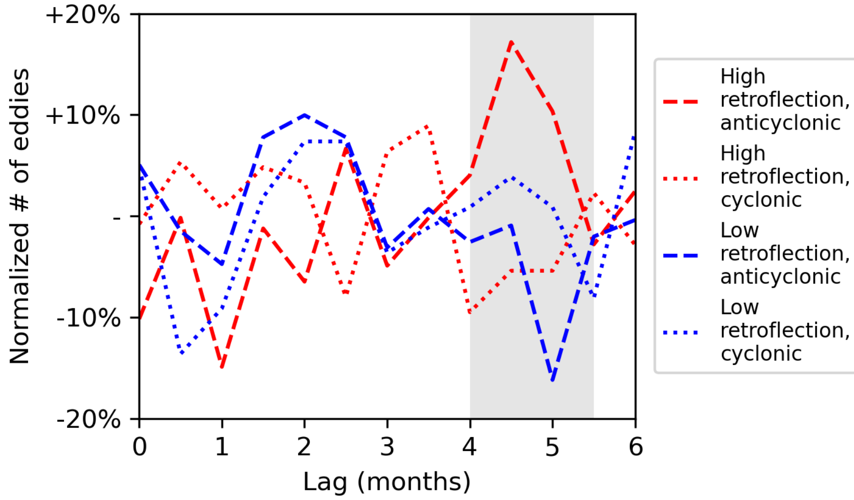

Figure S8: Anomalous number of eddies (in percentage) near the tip of the Grand Banks during strong (red) and weak (blue) retroflection periods based on the $\pm 1\sigma$ periods of the retroflection index. We differentiate cyclonic (dotted) and anti-cyclonic (dashed) features. The grey band indicates the expected lag between the retroflection index and the time when eddies are counted.

B Supplementary information on the method

Retroflection index

A small number of virtual particles that leave the Labrador Current at the Grand Banks flow neither west towards the Slope Sea or the eastern American continental shelf, nor east towards the subpolar North Atlantic; rather, they go south from the tip of the Grand Banks. These represent approximately 7% of the particles, and their number shows little variability with time. (Fig. S9 and *Jutras et al.*, *In prep*). Since these particles do not affect the retroflection index significantly and for the sake of simplicity, we count them as retroflected.

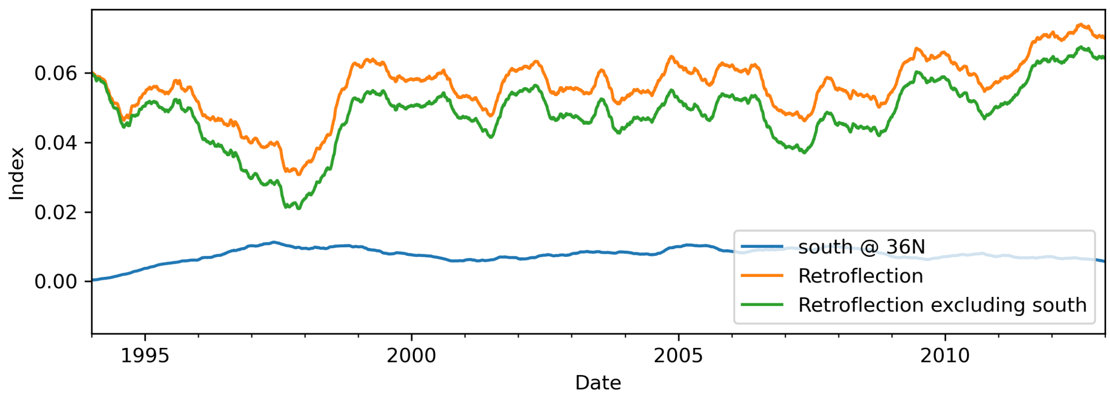

Figure S9: Timeseries of the number of particles going south from the Grand Banks (blue line), the retroflection index (orange line), and the retroflection index from which the particles going south are removed (green line).

In addition to the retroflection index based on Lagrangian trajectories, we compute a retroflection index based on an Eulerian approach. The Eulerian index is computed from the difference in the volume transport across the WB and SESPB sections (Fig. S16a). Whereas the Eulerian index represents the total transport, the Lagrangian index tracks only waters of subarctic origin. We therefore chose the Lagrangian index to study what controls the retroflection, but the two indices show a similar variability (not shown), and the Eulerian index is simpler to calculate.

Eliminated variables

During our analysis, we identified some variables that are not significantly correlated with the retroflection index. Whereas these results do not identify the forcing mechanisms at play, they help us understand what the main drivers are. The retroflection index has a low correlation with the freshwater transport. Furthermore, there is no clear relation between the retroflection index and the buoyancy fluxes, the mixed layer depths and convection along the shelf or in the Labrador Sea. This suggests that the dynamics of the system is the main determinant of the retroflection, while thermohaline processes play an indirect role, e.g. by affecting the strength of the transport.

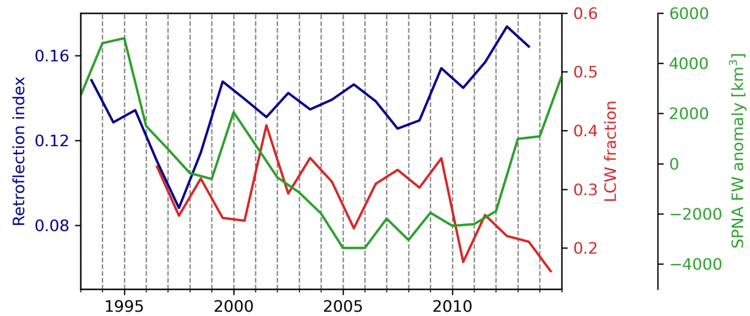

Figure S10: Time series of the Lagrangian retroflection index (dark blue), of the contributions of the Labrador Current Waters (LCW, red) to the deep waters at the mouth of the Laurentian Channel, on the 1027.3 kg m^{-3} isopycnal (*Jutras et al.*, 2020), and of the freshwater content anomaly in the upper 1000 m of the subpolar North Atlantic (green), reproduced with authorization from *Holliday et al.* (2020). The retroflection index is the yearly average of the smoothed time series.

The buoyancy fluxes across the air-sea interface are calculated as follows:

$$B = -\rho \left[\alpha \frac{Q}{c_p} - \beta S(E - P) \right] \tag{1}$$

where α and β are, respectively, the thermal expansion and the haline contraction coefficients, both functions of salinity and temperature, Q is the air-sea heat flux, c_p is the heat capacity of water, and $(E - P)$ is the net freshwater flux from the ocean, or evaporation minus precipitation, neglecting the river run-off as we are far from the coasts (*Gill*, 1982).

C Validations

Validation of the ocean reanalysis

The GLORYS12V1 outputs are evaluated against measurements of temperature, salinity and velocity provided by the Department of Fisheries and Oceans (DFO) Canada along selected hydrographic sections (*Cyr et al.*, 2020, see Fig. 1). A visual inspection shows that the values, location and timing of the fronts, both associated with the Gulf Stream and that separating the Labrador Shelf from the Labrador Sea, are generally consistent with observations (Fig. S11). GLORYS12V1 reproduces the main features seen in the observed velocity field, including the structure and direction of jets on the continental shelf and the location of the shelf-break jet. However, it underestimates the velocity of the shelf-break jet at the latitude of the SI section. The scarcity of the velocity data, with only one transect per summer, does not allow for a more quantitative estimate of this underestimation. The shelf-break jet is better resolved at lower latitudes, from the WB section downstream. Only the position of the NAC front at the SEGB section sometimes diverges from observations.

Comparison with trajectories of floats and drifters

The Lagrangian trajectories of virtual particles computed from the GLORYS12V1 ocean reanalysis are compared with trajectories of actual floats (Argo and RAFOS/SOFAR) and surface drifters.

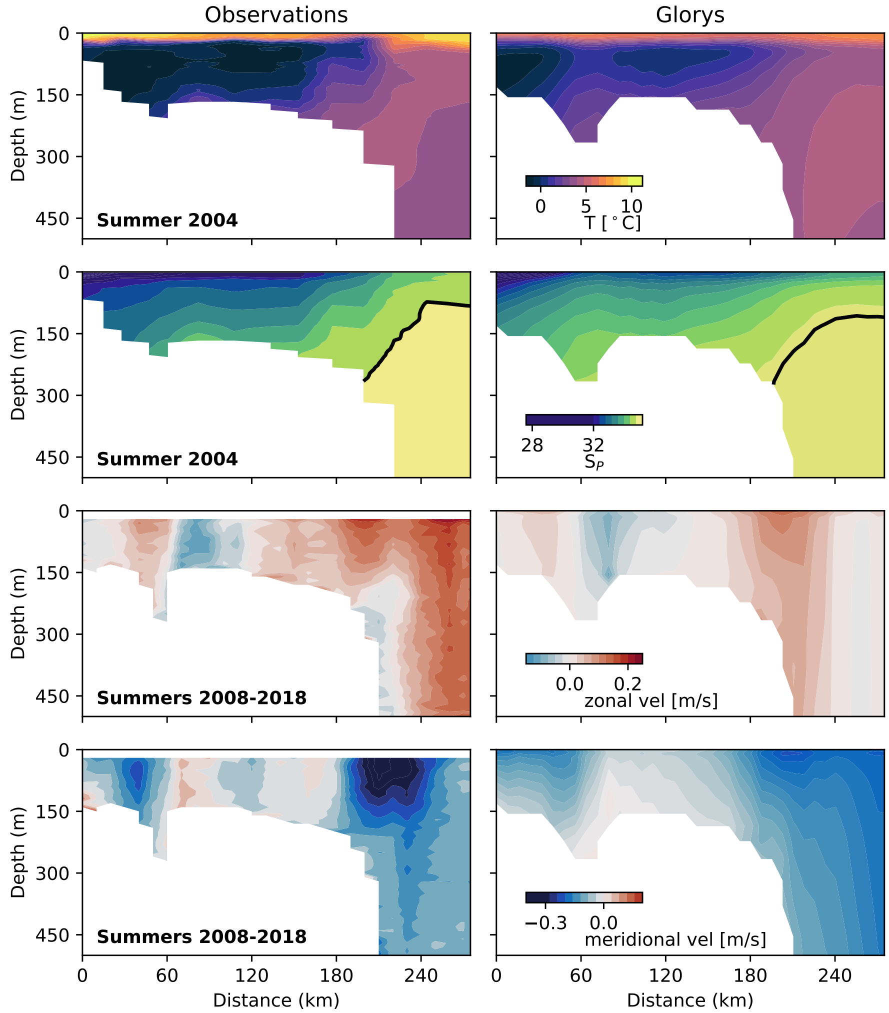

Figure S11: Comparison between DFO observations (left) and the GLORYS12V1 reanalysis (right) along the SI section (see Fig. S16a for the location of the hydrographic section). For temperature and salinity, observations from the 2004 sampling campaign are compared with the average values in summer 2004 in GLORYS12V1. For the zonal velocity and meridional velocity, we show the average of July months in 2008–2018. The black contour indicates the 34.8 salinity cut-off used to discriminate the Labrador Shelf waters from the Labrador Sea.

There are two important differences to note between the model-based and the observation-based trajectories. (1) Most of the Argo and RAFOS/SOFAR floats drift deeper than the virtual particles, and are thus advected by the Deep Western Boundary Current (see section Method). (2) While floats and drifters travel at a fixed depth, virtual particles can move vertically. Still, we use floats and drifters trajectories to perform a qualitative comparison with the virtual particle trajectories.

A visual inspection suggests the pathways of the floats/drifters and of the virtual particles generally agree (Fig. 1b,c). Furthermore, similarly to the virtual particles, two major pathways emerge from the observational dataset in the area of the Grand Banks: a westward pathway into the Slope Sea, and an eastward (retroflecting) pathway towards the subpolar North Atlantic. Overall, there is a rather limited number of observational platforms drifting in the area and period of interest (193 in total, starting in 2000, Fig. S13). This prevents us from performing a statistical analysis of the variability of the preferential pathway of these platforms. Nonetheless, we compare periods of weak retroflection (Fig S12, middle) and strong retroflection (Fig. S12, right) identified using the retroflection index. Since we only have observation-based trajectories starting from 2000 (Fig. S13), a comparison with the 1994-1996 weak retroflection period is impossible. In the periods of weak retroflection of 2003 and 2006-2007, 73 out of 90 floats and drifters (81%) retroflect, whereas 45 out of 49 (92%) retroflect during the periods of strong retroflection of 2009 and 2012-2016, qualitatively agreeing with what is found from the analysis of virtual particles. Moreover, the floats show similar behaviour compared to virtual particles in terms of interactions with eddies and meanders and the tip of the Grand Banks: some floats seem to be deviated by cyclonic eddies, while others are not (Fig. S14).

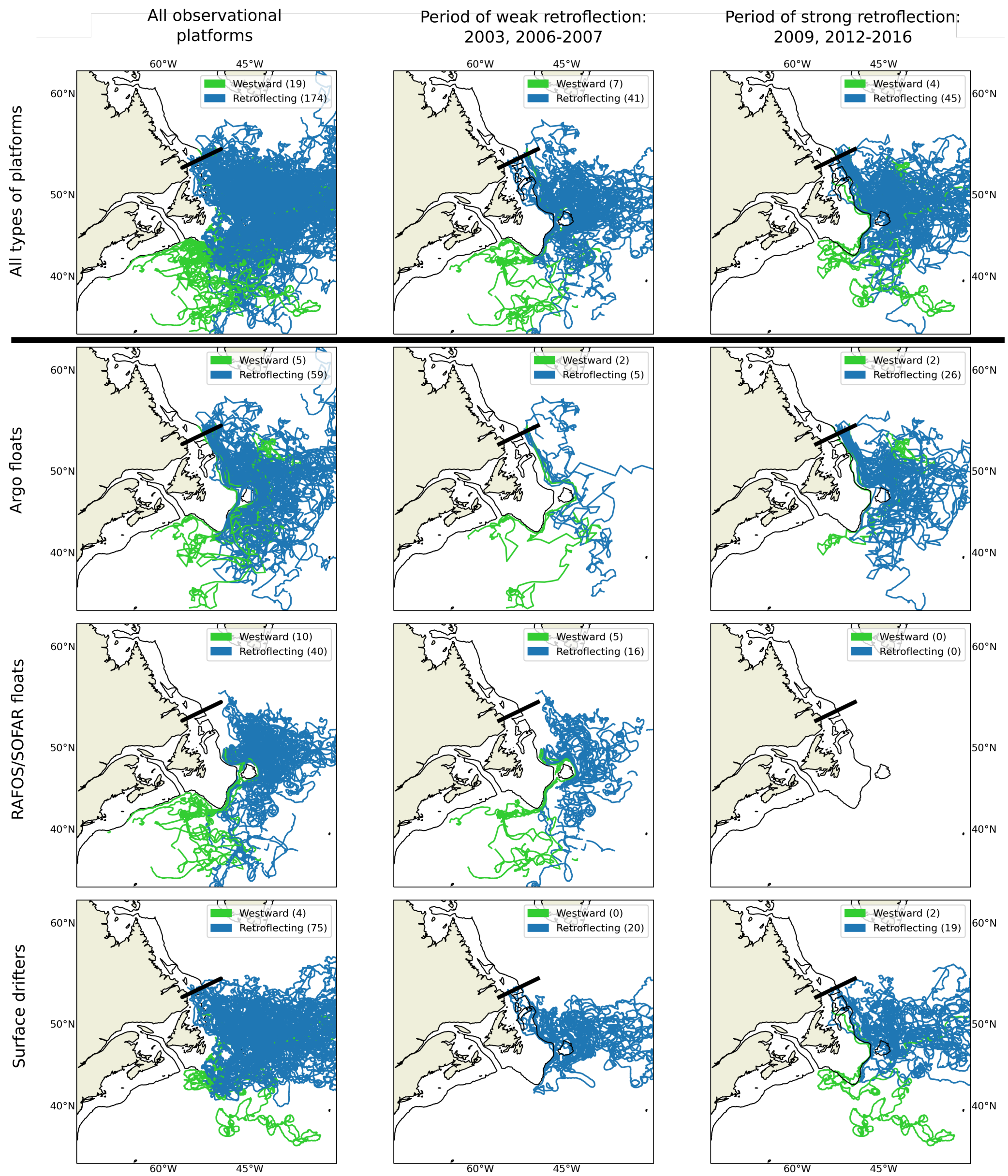

Figure S12: Observations from Argo floats (second row), RAFOS/SOFAR floats (third row) and surface drifters (bottom row) carried by the Labrador Current and passing through the Grand Banks region, in periods of weak (middle column) and strong (right column) retroflection identified from the retroflection index (see Fig. 3). The top row presents the three data types combined, and the left column the trajectories over the complete 1993-2018 period. The retroflected floats and drifters appear in blue, and the westward-flowing ones in green (see Fig. 1). The black and red lines show the hydrographic line that the platforms have to cross to be considered. The black contour delineates the 350 m isobath.

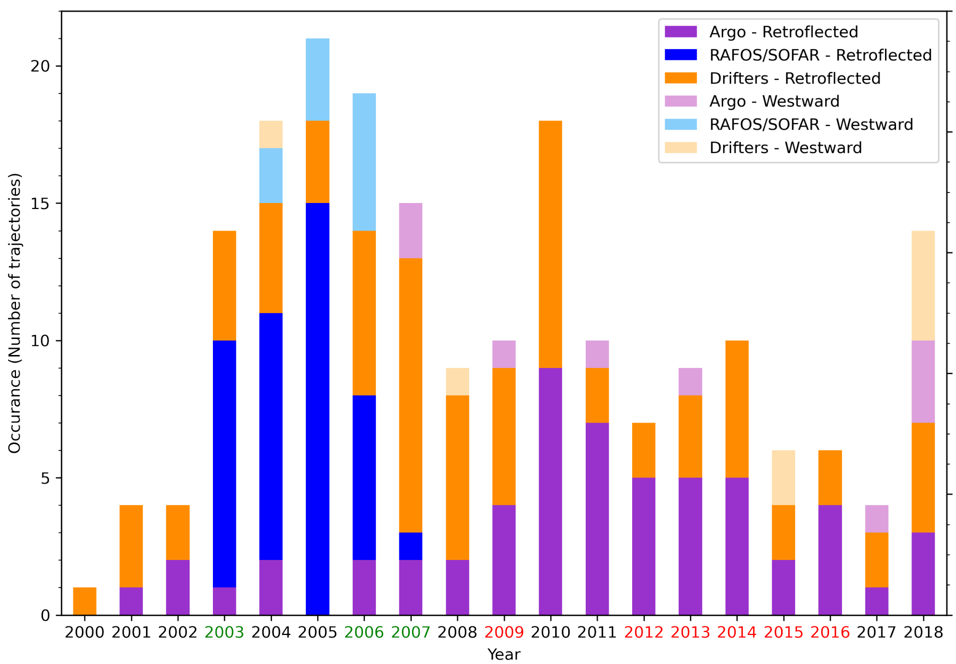

Figure S13: Distribution of floats and drifters over 2000–2018 categorized by float type: Argo floats (magenta), RAFOS and SOFAR floats (blue) and surface drifters (orange). The colour shading indicates if the floats retroflect (vivid) or move westward from the tip of the Grand Banks (dull). On the x-axis, years are identified as periods of weak (green) or strong (red) retroflection based on the retroflection index presented in Fig. 3.

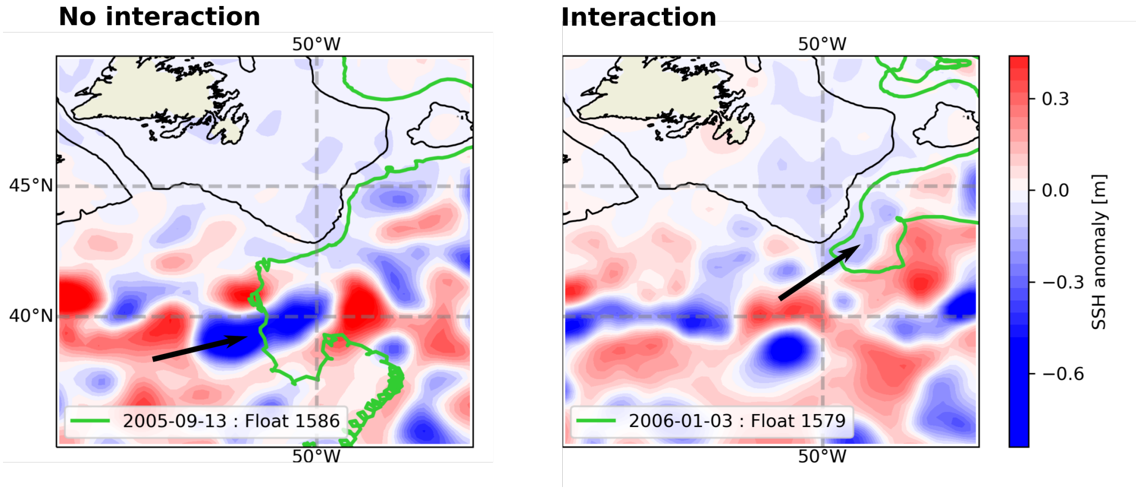

Figure S14: Similarly to Fig. 5, examples of situations that show (left) the absence of interaction between a float even in the present of eddies and (right) the deviation of a float by a cold-core (cyclonic) eddy. The black arrows point the eddies of interest. Both floats are RAFOS floats. The green line shows the trajectory of the float, and the colour shading indicates the sea level height anomaly at the time when the float reaches the tip of the Grand Banks, indicated in the legend along with the float number. The black line delineates the 350 m isobath.

D Labrador Current transport and circulation

Eulerian transport

In this section, we diagnose the volume transport and variability of the Labrador Current in the GLORYS12V1 reanalysis, and the coherence along its pathways. We compute the horizontal volume transport across various hydrographic sections monitored by DFO Canada on the Labrador Shelf, namely Seal Island (SI), White Bay (WB), Bonavista Bay (BB), Flemish Cap (FC), South-East Grand Banks (SEGB), South-East of St-Pierre Bank (SESPB), and Halifax Line (HL, see Fig. S16a). The outer edge of the section is chosen to cover the shelf-break jet. We find that the volume transport is weakly sensitive to small variations in the section edges.

The mean volume transport of the Labrador Current is 1.3 ± 0.2 (minimum of 0.6, maximum of 2.0) Sv on the Labrador Shelf (at the SI section) and 6.8 ± 1.0 (4.4–9.7) Sv for the shelf-break jet (Fig.S15). These numbers compare well with previous estimates from (*Petrie and Buckley*, 1996) of 6.3–9.8 Sv for total transport. At Flemish Cap, most of the current flows through the Flemish Pass, and only one quarter goes east around the Cap. As we move downstream, the Labrador Current progressively looses water offshore, and the total volume transport diminishes progressively (Fig. S15). Once the current reaches the Scotian Shelf (HL section), the mean volume transport drops to 0.6 ± 0.1 (0.1-1.0) Sv on the shelf and 1.3 ± 1.0 (0–4) Sv on the shelf-break.

The volume transport varies with time (Fig. S15). All along the shelf, the variance is of $\sim$ 0.1-0.2 Sv for the shelf component and of $\sim$1 Sv for the shelf-break component. Most of the variability follows a $\sim$6-year cycle on the Labrador Shelf, and around a 4-year cycle on the Scotian Shelf (from spectral analysis, not shown). The variability becomes less important in the last 10 years of the time series (2008-2018). There is a significant negative trend in the volume transport of the shelf-break branch all along the shelf ($\sim$-0.05 Sv yr^{-1}, Mann-Kendall test at 0.05 significance level), consistent with Fig. 3, and in the volume transport of the shelf branch south of the Flemish Cap ($\sim$-0.01 Sv yr^{-1}).

To better understand the circulation on the shelf, we investigate the coherence of the different branches and their interactions. To do so, for each branch, we correlate the time series of its volume transport, at different locations along its path. When looking at two points along the same path, a strong lagged correlation suggests that the current is not modified significantly from one location to the other. The transport of the shelf-break branch is coherent all along the Labrador Shelf (correlations $\sim$0.9, $p<0.001$). The transport is anti-correlated north and south of the Grand Banks, as reported by *Han et al.* (2014) (Fig. 3b). The shelf branch of the Labrador Current is somewhat coherent (correlations $\sim$0.5, $p<0.001$) on the Labrador Shelf and strongly coherent from Flemish Cap to the Scotian Shelf. The correlation is significant between the shelf and shelf-break branches in the Grand Banks area and south. This suggests that there are significant interactions between the two branches in that area. A summary of these results is illustrated in Fig. S16a.

External contribution to the Labrador Current

As the Labrador Current flows southward from subarctic regions, it receives freshwater discharge from the continent and exchanges water with the Labrador Sea and the NAC. Since computing the volume transport from velocities does not keep track of the origin of the water, by comparing the volume transport derived from the Eulerian framework and the one reconstructed from the volume carried by Lagrangian particles, we can estimate the "external" contributions to the Labrador Current. We find that these contributions are of the order of 2 Sv all along the shelf, with slight variations depending on the location (Fig. S16b). The subarctic waters' contribution to the Labrador Current diminishes dramatically as it flows south, reaching a few percents only on the Scotian Shelf. Given our interest in the fate of the fresh and well-oxygenated Labrador Shelf waters, the Lagrangian retroflection index is therefore more appropriate than the Eulerian index, as the latter contains the contributions from external sources.

Lagrangian trajectories

Whereas this paper focuses on the mechanisms leading to the retroflection of the Labrador Current, the Lagrangian trajectories we computed provide some interesting insights into the circulation of the area. Many of the particles seeded at intermediate depths (50-100 m) are upwelled to the surface layer by the time they reach Flemish Cap. Most of the particles take 0-1 month to reach the WB section, 2-3 months to reach the FC section, 4-7 months to reach the SESPB section, and 8-15 months (a larger spread) to reach the HL section. These times equate to an advection velocity along the Labrador shelf of $\sim$7-11 cm s^{-1}. In comparison, *Lazier and Wright* (1993) measured velocities of 6-23 cm s^{-1} in the Labrador Current, and *Fratantoni and McCartney* (2010) and *Petrie et al.* (1991) found an advection velocity of $\sim$20 cm s^{-1} by tracking salinity anomalies.

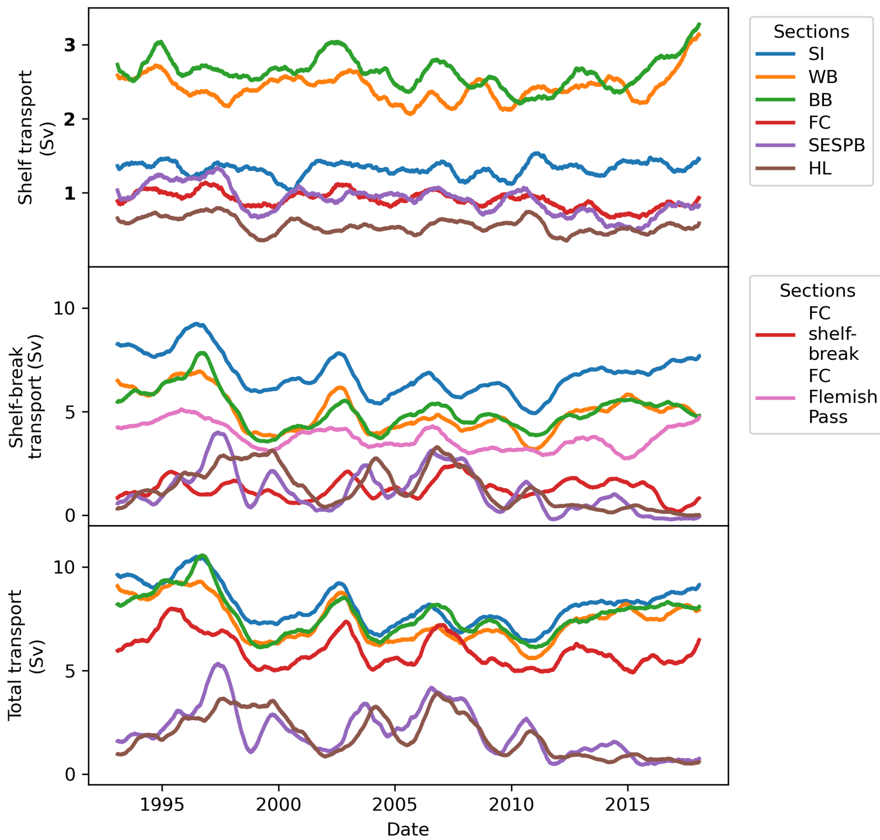

Figure S15: Time series of volume transport, computed from an Eulerian approach, on the shelf (top), at the shelf-break (middle), and over both (bottom), at different sections, smoothed with a one-year moving average. For the location of the sections and the indication of the separation point between the shelf and shelf-break components, see Fig. S16a.

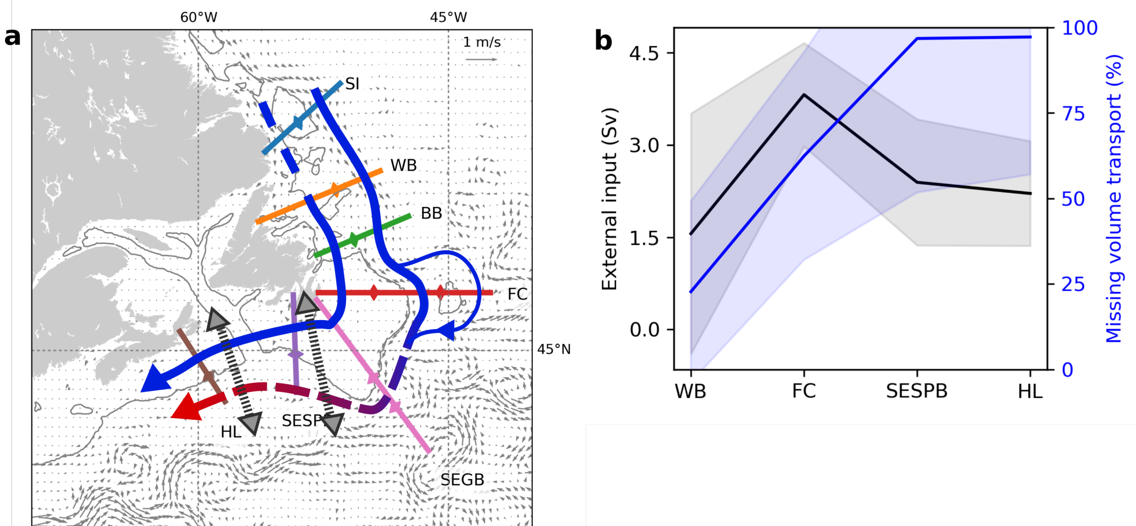

Figure S16: **(a)** Coherence within and interactions between branches of the Labrador Current. A full line indicates a high coherence of the branch (strongly correlated with upstream), a dashed line some coherence. The color indicates the sign of the correlation. The switch from blue to red in the shelf-break branch indicates that the transport along the Scotian Shelf is anti-correlated with that along the Labrador Shelf. The fine dashed grey lines indicate locations of interactions between the shelf and shelf-break branches. Sections (straight lines) and separation points (diamonds) between the shelf and the shelf-break are shown. The light grey arrows in the background provide a snapshot of the current speed averaged over the top 1000 m, or down to the seafloor if it is shallower than 1000 m. **(b)** In black: "external" contributions (not originating from the subarctic) to the Labrador Current, computed from the difference between the Eulerian and Lagrangian volume transport, at different sections. In blue: cumulative contribution (in percentage) of "external" contributions to the total volume transport across each section. The shaded area shows the standard deviation associated with the time series.

References

Cyr, F., E. Colbourne, P. S. Galbraith, O. Gibb, S. Snook, C. Bishop, N. Chen, G. Han, and D. Senciall, Physical Oceanographic Conditions on the Newfoundland and Labrador Shelf during 2018, *DFO Can.Sci. Advis. Sec. Res. Doc.*, p. 48 pp., 2020.

Fratantoni, P. S., and M. S. McCartney, Freshwater export from the Labrador Current to the North Atlantic Current at the Tail of the Grand Banks of Newfoundland, *Deep-Sea Research Part I: Oceanographic Research Papers*, *57*(2), 258–283, doi:10.1016/j.dsr.2009.11.006, 2010.

Gill, A. E., Transfer of Properties between Atmosphere and Ocean, in *Atmosphere—Ocean Dynamics*, vol. 30, chap. 2, pp. 19–38, Academic Press, doi:10.1016/S0074-6142(08)60027-3, 1982.

Han, G., N. Chen, and Z. Ma, Is there a north-south phase shift in the surface Labrador Current transport on the interannual-to-decadal scale?, *Journal of Geophysical Research: Oceans*, *119*(1), 276–287, doi:10.1002/2013JC009102, 2014.

Holliday, N. P., et al., Ocean circulation causes the largest freshening event for 120 years in eastern subpolar North Atlantic, *Nature Communications*, *11*(1), doi:10.1038/s41467-020-14474-y, 2020.

Jutras, M., N. Planat, and C. O. Dufour, Unsupervised clustering of oceanic Lagrangian particles: identification of the main pathways of the Labrador Current.

Jutras, M., C. O. Dufour, A. Mucci, F. Cyr, and D. Gilbert, Temporal Changes in the Causes of the Observed Oxygen Decline in the St. Lawrence Estuary, *Journal of Geophysical Research: Oceans*, *125*(12), 1–20, doi:10.1029/2020JC016577, 2020.

Lazier, J. R. N., and D. G. Wright, Annual velocity variations in the Labrador Current, *Journal of Physical Oceanography*, *23*(4), 659–678, doi:10.1175/1520-0485(1993)023<0659:AVVITL>2.0.CO;2, 1993.

Petrie, B. D., and J. Buckley, Volume and freshwater transport of the Labrador Current in Flemish Pass, *Journal of Geophysical Research C: Oceans*, *101*(C12), 28,335–28,342, doi:10.1029/96JC02779, 1996.

Petrie, B. D., S. Akenhead, and J. R. N. Lazier, Temperature and salinity variability on the eastern newfoundland shelf: The annual harmonic, *Atmosphere - Ocean*, *29*(1), 14–36, doi:10.1080/07055900.1991.9649390, 1991.